Effects of Pressure and Temperature on the Self-Assembled Fully Hydrated Nanostructures of Monoolein−Oil Systems

ARTICLE *in* LANGMUIR · SEPTEMBER 2009

Impact Factor: 4.46 · DOI: 10.1021/la9023019 · Source: PubMed

Langmuir
Article
pubs.acs.org/Langmuir

Effects of Pressure and Temperature on the Self-Assembled Fully Hydrated Nanostructures of Monoolein−Oil Systems

Anan Yaghmur,*[,†,§] Manfred Kriechbaum,[†] Heinz Amenitsch,[†] Miloš Steinhart,[‡] Peter Laggner,[†] and Michael Rappolt[†]

[†]*Institute of Biophysics and Nanosystems Research (IBN), Austrian Academy of Sciences, Graz, Austria, and* [‡]*Institute of Macromolecular Chemistry, Academy of Sciences of the Czech Republic, Prague, Czech Republic.* [§] *Permanent address: Department of Pharmaceutics and Analytical Chemistry, Faculty of Pharmaceutical Sciences, University of Copenhagen, Universitetsparken 2, DK-2100 Copenhagen, Denmark.*

Received June 26, 2009. Revised Manuscript Received July 30, 2009

Synchrotron small-angle X-ray scattering (SAXS) was applied for studying the effects of hydrostatic pressure and temperature on the structural behavior of fully hydrated tetradecane (TC)-loaded monoolein (MO) systems. Our main attention focused on investigating the impact of isobaric and isothermal changes on the stability of the inverted type discontinuous *Fd*3*m* cubic phase as compared to the inverted type hexagonal (H_2) liquid crystalline phase. The present results show that compressing the TC-loaded *Fd*3*m* phase under isothermal conditions induces a significant increase of its lattice parameter: it approximately increases by 1 Å per 75 bar. Further, the *Fd*3*m* phase is more pressure-sensitive as compared to the *Pn*3*m* and the H_2 phases. At ambient temperatures, we observed the following structural transitions as pressure increases: *Fd*3*m* → H_2 → *Pn*3*m*. Our findings under isobaric conditions reveal more complicated structural transitions. At high pressures, we recorded the interesting temperature-induced structural transition of (*Pn*3*m* + L_α) → (*Pn*3*m* + L_α + H_2) → (L_α + H_2) → H_2 → *Fd*3*m* → traces of *Fd*3*m* coexisting with L_2. At high pressures and low temperatures, the TC molecules partially crystallize as indicated by the appearance of an additional diffraction peak at q = 3.46 nm^{-1}. This crystallite disappears at high temperatures and also as the system gets decompressed. The appearance of the *Pn*3*m* and the L_α phases during compressing the fully hydrated MO/TC samples at high pressures and low temperatures is generally related to a growing hydrocarbon chain condensation, which leads to membrane leaflets with less negative interfacial curvatures (decreasing the spontaneous curvatures $|H_0|$). Both the effects of pressure and temperature are discussed in detail for all nonlamellar phases on the basis of molecular shape and packing concepts.

Introduction

Lyotropic liquid crystalline phases originating from the self-assembly of biologically relevant lipids in water are hierarchical complex assemblies. Their nanostructures are tunable and strongly depend on hydration level, lipid molecular structure, and composition and depend of course on the experimental conditions.[1−7] Among the experimental parameters, several reports on modulating the nanostructure by varying pressure,[3,8−17] temperature,[1,2,5,7,18−21] and pH value[22] were published. It has also been demonstrated that salt concentration,[23,24] the presence of peptides,[25−27] and proteins[28−30] play a vital role in controlling the lipid-based nanostructures. The one-dimensional (1D) lamellar (L_α), the two-dimensional (2D) inverted hexagonal (H_2), and the three-dimensional (3D) reversed bicontinuous (V_2) or discontinuous

*Corresponding author: Tel +45 35 33 65 41, Fax +45 35336030, e-mail aya@farma.ku.dk.

(1) Kaasgaard, T.; Drummond, C. J. *Phys. Chem. Chem. Phys.* **2006**, *8*, 4957–4975.
(2) Qiu, H.; Caffrey, M. *Biomaterials* **2000**, *21*, 223–234.
(3) Conn, C. E.; Ces, O.; Mulet, X.; Finet, S.; Winter, R.; Seddon, J. M.; Templer, R. H. *Phys. Rev. Lett.* **2006**, *96*, 108102.
(4) Duesing, P. M.; Seddon, J. M.; Templer, R. H.; Mannock, D. A. *Langmuir* **1997**, *13*, 2655–2664.
(5) de Campo, L.; Yaghmur, A.; Sagalowicz, L.; Leser, M. E.; Watzke, H.; Glatter, O. *Langmuir* **2004**, *20*, 5254–5261.
(6) Yaghmur, A.; de Campo, L.; Sagalowicz, L.; Leser, M. E.; Glatter, O. *Langmuir* **2006**, *22*, 9919–9927.
(7) Czeslik, C.; Winter, R.; Rapp, G.; Bartels, K. *Biophys. J.* **1995**, *68*, 1423–1429.
(8) Winter, R. *Curr. Opin. Colloid Interface Sci.* **2001**, *6*, 303–312.
(9) Daniel, I.; Oger, P.; Winter, R. *Chem. Soc. Rev.* **2006**, *35*, 858–875.
(10) Seddon, J. M.; Squires, A. M.; Conn, C. E.; Ces, O.; Heron, A. J.; Mulet, X.; Shearman, G. C.; Templer, R. H. *Philos. Trans. R. Soc. London., Ser. A* **2006**, *364*, 2635–2655.
(11) Winter, R.; Erbes, J.; Templer, R. H.; Seddon, J. M.; Syrykh, A.; Warrender, N. A.; Rapp, G. *Phys. Chem. Chem. Phys.* **1999**, *1*, 887–893.
(12) Pisani, M.; Bernstorff, S.; Ferrero, C.; Mariani, P. *J. Phys. Chem. B* **2001**, *105*, 3109–3119.
(13) Pisani, M.; Narayanan, T.; Di Gregorio, G. M.; Ferrero, C.; Finet, S.; Mariani, P. *Phys. Rev. E* **2003**, *68*, 021924.
(14) Winter, R.; Kohling, R. *J. Phys.: Condens. Matter.* **2004**, *16*, S327–S352.
(15) Winter, R. *Biochim. Biophys. Acta, Protein Struct. Mol. Enzymol.* **2002**, *1595*, 160–184.
(16) Winter, R.; Erbes, J.; Czeslik, C.; Gabke, A. *J. Phys.: Condens. Matter* **1998**, *10*, 11499–11518.
(17) So, P. T. C.; Gruner, S. M.; Erramilli, S. *Phys. Rev. Lett.* **1993**, *70*, 3455–3458.
(18) Dong, Y. D.; Larson, I.; Hanley, T.; Boyd, B. J. *Langmuir* **2006**, *22*, 9512–9518.
(19) Misquitta, Y.; Caffrey, M. *Biophys. J.* **2001**, *81*, 1047–1058.
(20) Rappolt, M.; Hickel, A.; Bringezu, F.; Lohner, K. *Biophys. J.* **2003**, *84*, 3111–3122.
(21) Hartley, P. G.; Alderton, M. R.; Dawson, R. M.; Wells, D. *Bioconjugate Chem.* **2007**, *18*, 152–159.
(22) Okamoto, Y.; Masum, S. M.; Miyazawa, H.; Yamazaki, M. *Langmuir* **2008**, *24*, 3400–3406.
(23) Awad, T. S.; Okamoto, Y.; Masum, S. M.; Yamazaki, M. *Langmuir* **2005**, *21*, 11556–11561.
(24) Yaghmur, A.; Laggner, P.; Sartori, B.; Rappolt, M. *PLoS ONE* **2008**, *3*, e2072.
(25) Kamo, T.; Nakano, M.; Kuroda, Y.; Handa, T. *J. Phys. Chem. B* **2006**, *110*, 24987–24992.
(26) Yaghmur, A.; Laggner, P.; Zhang, S.; Rappolt, M. *PLoS ONE* **2007**, *2*, e479.
(27) Siegel, D. P.; Cherezov, V.; Greathouse, D. V.; Koeppe, R. E.; Killian, J. A.; Caffrey, M. *Biophys. J.* **2006**, *90*, 200–211.
(28) Kraineva, J.; Smirnovas, V.; Winter, R. *Langmuir* **2007**, *23*, 7118–7126.
(29) Kraineva, J.; Nicolini, C.; Thiyagarajan, P.; Kondrashkina, E.; Winter, R. *Biochim. Biophys. Acta, Proteins Proteomics* **2006**, *1764*, 424–433.
(30) Rizwan, S. B.; Hanley, T.; Boyd, B. J.; Rades, T.; Hook, S. *J. Pharm. Sci.*, in press.

cubic (I_2) liquid crystalline phases are examples of these complexes that mimic highly ordered lipidic domains observed in biomembranes.[31,32] Recently, Shearman et al.[33] reported on the formation of a novel 3D hexagonal reversed micellar system of the symmetry $P6_3/mmc$ consisting of identical spherical micelles.

The lamellar−nonlamellar structural transitions in model surfactant-like lipid systems have also sparked great interest owing to the fundamental importance of these transitions in modulating the physicochemical properties of biomembranes.[32,34,35] They play a crucial role in the regulation of different biological processes such as membrane fusion and fat digestion.[34]

Within the range of self-assembled phases in model surfactant-like lipid systems, the monoglyceride-based lyotropic liquid crystalline phases are relatively unique owing to their rich polymorphism in water[2,5,7,19,36] and the potential application as drug nanocarriers.[37−39] Various studies have focused on understanding their self-assembly behavior,[2,5,36] studying the effects of loading hydrophilic or hydrophobic guest molecules,[39−41] and exploring the impact of varying temperature[2,3,5,7] or pressure.[3,7,12] Among these monoglycerides, monoolein[2,7,12,42,43] (MO) and monolinolein[5,6,40,44] (MLO) are well studied. They self-assemble in water to form various well-ordered inverted type nanostructures: a fluid isotropic micellar solution (L_2), L_α, H_2, and V_2 phases. In addition, much effort has been devoted in the past two decades to form various nanostructured aqueous dispersions with these model lipids such as cubosomes, hexosomes, and micellar cubosomes by confining with suitable stabilizers the corresponding fully hydrated crystalline phases in kinetically submicrometer sized particles.[5,18,45−49]

Daniel et al.[9] described in a recent review different pressure-dependent processes and gave particular interest in high-pressure effects on different biologically relevant systems. Typical examples are the pressure-induced lipid bilayer−peptide (or −protein) interactions and unfolding kinetics of proteins.[9] For the fully hydrated lyotropic liquid crystalline phases, the pressure variations significantly influence the lipid membranes and the lipid phase transitions.[3,7,10,12]

It is clear that understanding the pressure- and temperature-induced structural transitions for lipid/oil mixtures in excess water would require a detailed consideration of a complex set of interactions, since lipid−lipid, lipid−oil, lipid−water, and lipid−oil−water interactions are involved.[7,12] In this context, the pressure and temperature structural transitions strongly depend on different parameters such as the molecular structure of the lipid[3,5,7,36,48] (single or double chained, headgroup, saturation degree, and length of fatty acyl chain), the presence of hydrophilic or hydrophobic additives,[40,50] and electrostatic effects.[23,24] In general, the behavior of pressure-dependent structural transitions displays opposite trends in lipid systems as compared to the influence of temperature.[4,10,17] However, it is important noting that the effects of pressure and temperatures on these nanostructures are not congruent.[3,4,10] It is obvious from previous studies[3,4,7] that increasing pressure favors the formation of the V_2 phases, and conversely it tends to destabilize phases with high packing costs[51] such as the discontinuous micellar cubic phase of the symmetry *Fd3m*.

In the present study, we focus on the effect of the hydrostatic pressure at different temperatures on oil loaded MO-based systems. Our main objective addresses the effect of pressure variation on the stability of both *Fd3m* and H_2 phases under high-pressure conditions, and their pressure- and temperature-dependent phase behaviors have also been explored. The pressure−temperature effects on the oil-loaded *Fd3m* phase are of particular interest, since to date only few experimental studies have been carried out on the pressure dependence of this phase, e.g., on fully hydrated glycolipid systems.[4,52] An investigation of the impact of pressure on ternary oil-loaded discontinuous cubic phases should lead to an improved understanding of the behavior of this interesting phase at high pressures. We used synchrotron small-angle X-ray scattering (SAXS) to analyze the pressure-induced structural transitions in two fully hydrated MO/TC/water systems at fixed MO/TC weight ratios of 7/3 (sample A) and 6/4 (sample B), respectively.

Materials and Methods

Materials. Monoolein (1-monooleoyl-*rac*-glycerol, MO, purity: 99%) was purchased from Sigma Chemical Co. (St. Louis, MO). Chloroform ($CHCl_3$, purity >99%) was supplied by Carl Roth GmbH (Karlsruhe, Germany). Tetradecane (TC) was obtained from Sigma Chemical Co. (St. Louis, MO). The used buffer was PBS (phosphate buffered saline contains 20 mM NaPi and 130 mM NaCl, pH 7.4). All ingredients were used without further purification.

Preparation of MO/TC Bulk Samples. Two MO/TC mixtures at appropriate weight ratios were dissolved in chloroform. This solvent was then evaporated using a gentle stream of nitrogen, followed by drying under vacuum for at least 12 h in order to remove completely the residual organic solvent. The dry lipid film was hydrated by adding the PBS buffer and carrying out at least five freeze−thaw cycles between liquid nitrogen and room temperature and then homogenizing several times during the thawing steps by vigorous vortexing. These fully hydrated samples in excess water were formed with a fixed total lipid (MO) plus oil concentration of 30 wt %. The used oil was TC. The two ternary systems (samples A and B) were formed with MO/TC weight ratios of 7/3 and 6/4, respectively. The prepared samples were incubated at room temperature for two to 3 weeks before carrying out SAXS measurements.

(31) Almsherqi, Z.; Hyde, S.; Ramachandran, M.; Deng, Y. *J. R. Soc. Interface* **2008**, *5*, 1023–1029.
(32) Almsherqi, Z. A.; Kohlwein, S. D.; Deng, Y. *J. Cell Biol.* **2006**, *173*, 839–844.
(33) Shearman, G. C.; Tyler, A. I.; Brooks, N. J.; Templer, R. H.; Ces, O.; Law, R. V.; Seddon, J. M. *J. Am. Chem. Soc.* **2009**, *131*, 1678–1679.
(34) Patton, J. S.; Carey, C. M. *Science* **1979**, *204*, 145–148.
(35) Landh, T. *FEBS Lett.* **1995**, *369*, 13–17.
(36) Barauskas, J.; Landh, T. *Langmuir* **2003**, *19*, 9562–9565.
(37) Shah, J. C.; Sadhale, Y.; Chilukuri, D. M. *Adv. Drug Delivery Rev.* **2001**, *47*, 229–250.
(38) Fong, W. K.; Hanley, T.; Boyd, B. J. *J. Controlled Release* **2009**, *135*, 218–226.
(39) Drummond, C. J.; Fong, C. *Curr. Opin. Colloid Interface Sci.* **1999**, *4*, 449–456.
(40) Yaghmur, A.; de Campo, L.; Sagalowicz, L.; Leser, M. E.; Glatter, O. *Langmuir* **2005**, *21*, 569–577.
(41) Murgia, S.; Caboi, F.; Monduzzi, M. *Chem. Phys. Lipids* **2001**, *110*, 11–17.
(42) Rappolt, M.; Di Gregorio, G. M.; Almgren, M.; Amenitsch, H.; Pabst, G.; Laggner, P.; Mariani, P. *Europhys. Lett.* **2006**, *75*, 267–273.
(43) Conn, C. E.; Ces, O.; Squires, A. M.; Mulet, X.; Winter, R.; Finet, S. M.; Templer, R. H.; Seddon, J. M. *Langmuir* **2008**, *24*, 2331–2340.
(44) Yaghmur, A.; de Campo, L.; Salentinig, S.; Sagalowicz, L.; Leser, M. E.; Glatter, O. *Langmuir* **2006**, *22*, 517–521.
(45) Gustafsson, J.; Ljusberg-Wahren, H.; Almgren, M.; Larsson, K. *Langmuir* **1996**, *12*, 4611–4613.
(46) Gustafsson, J.; Ljusberg-Wahren, H.; Almgren, M.; Larsson, K. *Langmuir* **1997**, *13*, 6964–6971.
(47) Larsson, K. *Curr. Opin. Colloid Interface Sci.* **2009**, *14*, 16–20.
(48) Yaghmur, A.; Laggner, P.; Almgren, M.; Rappolt, M. *PLoS ONE* **2008**, *3*, e3747.
(49) Yaghmur, A.; Glatter, O. *Adv. Colloid Interface Sci.* **2009**, *147−148*, 333–342.
(50) Caboi, F.; Amico, G. S.; Pitzalis, P.; Monduzzi, M.; Nylander, T.; Larsson, K. *Chem. Phys. Lipids* **2001**, *109*, 47–62.
(51) Shearman, G. C.; Ces, O.; Templer, R. H.; Seddon, J. M. *J. Phys.: Condens. Matter* **2006**, *18*, S1105–S1124.
(52) Seddon, J. M.; Robins, J.; Gulik-Krzywicki, T.; Delacroix, H. *Phys. Chem. Chem. Phys.* **2000**, *2*, 4485–4493.

Time-Resolved Synchrotron X-ray Scattering Measurements. X-ray scattering patterns were recorded at the Austrian SAXS beamline[53] (camera length 125 cm) at the synchrotron light source ELETTRA (Trieste, Italy) using a one-dimensional position sensitive detector (Gabriel type), which covered the q-range ($q = 4\pi \sin\theta/\lambda$, where λ is the wavelength and 2θ is the scattering angle) of interest from about $2\pi/87$ to $2\pi/1.4$ nm^{-1} at an X-ray energy of 8 keV. Silver behenate ($CH_3-(CH_2)_{20}-COOAg$) with a d spacing value of 5.84 nm was used as a standard to calibrate the angular scale of the measured intensity.

For the high-pressure experiments, we have utilized a high-pressure X-ray cell,[54,55] where the X-ray scattering experiments can be performed under hydrostatic pressures up to 3 kbar, and the samples can be thermostated with a water bath between −20 and +80 °C (stability ±0.1 °C, Unistat CC, Huber, Offenburg, Germany). The computer-aided pressure adjustment had a calibrated precision of ±0.5%, and the temperature was computer-controlled to a precision of ±0.1 °C. Pressures up to 1.5 kbar were produced by a motor-driven, piston-type generator by compressing water (low compressibility) and by transmitting it via a high-pressure network into the sample cell. The cell had two diamond windows with a thickness of either 0.75 mm leaving a free optical path length of 3 mm and allowing scattering to be observed at angles up to 30°. The samples (less than 30 μL) were filled in a capsule of cylindrical shape (length 3 mm, diameter 3 mm) made of aluminum, sealed at both ends with a mylar foil of 100 μm thickness, in order to avoid contamination or dilution with the pressurizing medium water, and inserted into the high-pressure cell. All functions of the experimental setup (temperature, pressure, scan rate) were personal computer controlled and synchronized with the X-ray data acquisition (number of diffraction frames, exposure times). Further details and applications of the pressure cell are given in a previous report.[56]

X-ray Data Analysis. In the time-resolved X-ray scattering experiments, the lattice spacings of the L_α, the H_2, the discontinuous *Fd3m* cubic, and the bicontinuous *Pn3m* cubic phases were derived from the SAXS diffraction pattern by standard procedures as described in a recent review.[57] In short, after the raw data had been corrected for detector efficiency and the background scattering from both water and the sample cell had been subtracted, all Bragg peaks were fitted by Lorentzian distributions. We note that in each respective phase regime only the strongest reflections were considered. The fittings were carried out with home written procedures running under IDL 5.2 (ITT Visual Information Solutions, Boulder, CO).

Results and Discussion

1. Pressure-Induced Isothermal Tuning of Curvatures of Oil-Containing MO Systems. In this section, SAXS experiments are presented, which were carried out on sample A (an oil-loaded fully hydrated MO system) at selected temperatures as a function of pressure. Figure 1a shows the typical structural transitions observed at 20 °C as pressure increases in the range of 1−1200 bar. At 1 bar, the self-assembled *Fd3m* phase in excess water is identified by recording the first 13 reflections, in which the strongest ones were used for the lattice parameter determination. A typical example for the indexing is illustrated in Figure 2. This cubic phase consists of an 3D periodically ordered complex. It is

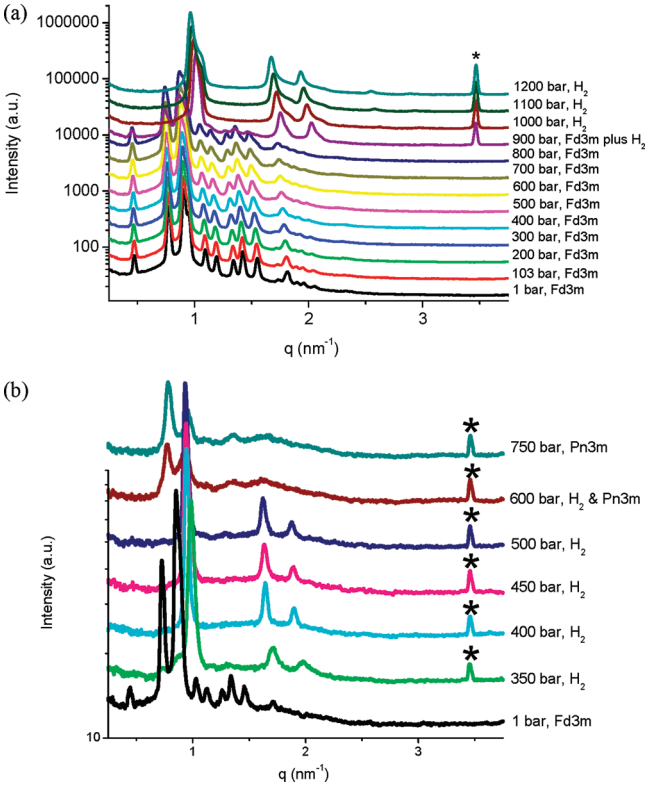

Figure 1. Pressure-dependence behavior of sample A at two different temperatures. (a) At 20 °C in a pressure range from 1 to 1200 bar the SAXS scattering patterns reveal the structural transitions from the *Fd3m* via a biphasic system of *Fd3m* coexisting with H_2 to the H_2 phase. (b) At 7 °C in a pressure range from 1 to 700 bar, the *Fd3m* phase undergoes a transition to H_2 phase and via a coexistence of the H_2 and *Pn3m* phases to the pure *Pn3m* phase. At high pressures and low temperatures, an additional peak generally appears at a high q value. It is marked in this figure (and also in the next figures) with an asterisk and indicates the partial crystallization of TC molecules. The scattering curves are shifted by an arbitrary constant for better visibility.

packing two different types of discrete inverse micelles, both quasi-spherical.[52,58−62] In this phase, the unit cell contains 8 larger inverse micelles[58−60,62] of symmetry $\overline{4}3m$ arranged tetrahedrally on a diamond lattice and 16 smaller reverse micelles of symmetry $\overline{3}m$. The core of these micelles consists of hydrophilic aqueous domains (water plus the headgroups of the lipid molecules) and continuous three-dimensional oleic medium (oil plus the hydrophobic tails of the lipid molecules). In the literature, previous studies reported on the formation of the *Fd3m* cubic phase in the ternary systems of (phosphatidylcholine/fatty alcohols/water)[63] and (phosphatidylcholine/diacylglycerol/water),[58] in the binary glycolipid/water systems,[4,52,62,64] and in the ternary MLO/TC/water system.[44] This micellar cubic phase was also observed in a ternary mixture[65] of amphiphilic diblock copolymer/oil/water. It should be pointed out that previous investigations on the

(53) Amenitsch, H.; Rappolt, M.; Kriechbaum, M.; Mio, H.; Laggner, P.; Bernstorff, S. *J. Synchrotron Radiat.* **1998**, *5*, 506–508.
(54) Pressl, K.; Kriechbaum, M.; Steinhart, M.; Laggner, P. *Rev. Sci. Instrum.* **1997**, *68*, 4588–4592.
(55) Steinhart, M.; Kriechbaum, M.; Pressl, K.; Amenitsch, H.; Laggner, P.; Bernstorff, S. *Rev. Sci. Instrum.* **1999**, *70*, 1540–1545.
(56) Rappolt, M.; Amenitsch, H.; Strancar, J.; Teixeira, C. V.; Kriechbaum, M.; Pabst, G.; Majerowicz, M.; Laggner, P. *Adv. Colloid Interface Sci.* **2004**, *111*, 63–77.
(57) Rappolt, M. In *Planar Lipid Bilayers and Liposomes*; Leitmannova, A., Ed.; Elsevier: Amsterdam, 2006; Vol. *5*, p 253.
(58) Seddon, J. M. *Biochemistry* **1990**, *29*, 7997–8002.
(59) Luzzati, V.; Vargas, R.; Gulik, A.; Mariani, P.; Seddon, J. M.; Rivas, E. *Biochemistry* **1992**, *31*, 279–285.
(60) Delacroix, H.; Gulik-Krzywicki, T.; Seddon, J. M. *J. Mol. Biol.* **1996**, *258*, 88–103.
(61) Duesing, P. M.; Templer, R. H.; Seddon, J. M. *Langmuir* **1997**, *13*, 351–359.
(62) Minamikawa, H.; Hato, M. *Langmuir* **1998**, *14*, 4503–4509.
(63) Huang, Z.; Seddon, J. M.; Templer, R. H. *Chem. Phys. Lipids* **1996**, *82*, 53–61.
(64) Seddon, J. M.; Zeb, N.; Templer, R. H.; McElhaney, R. N.; Mannock, D. A. *Langmuir* **1996**, *12*, 5250–5253.
(65) Alexandridis, P.; Olsson, U.; Lindman, B. *Langmuir* **1996**, *12*, 1419–1422.

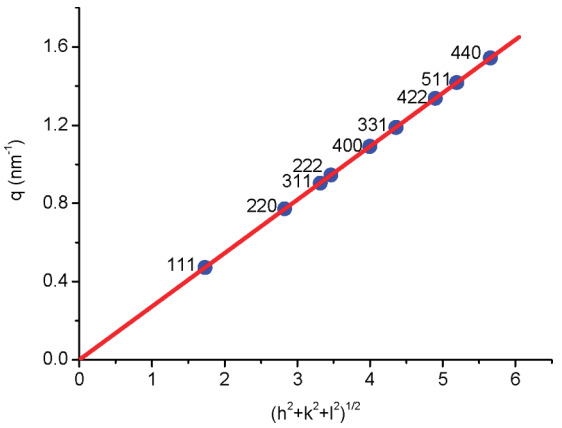

Figure 2. Indexing of the *Fd3m* diffraction pattern of sample A at 20 °C and 1 bar. A linear relationship of the q values of the observed peaks versus $(h^2 + k^2 + l^2)^{1/2}$ is given. From the linear fit (full line), the lattice spacing $a = 23.04$ nm is determined.

temperature-dependent behavior of both binary MO/water[2,7] and MLO/water systems[5] did not show any evidence for the formation of the *Fd3m* phase.

As shown in Figure 1a, up to 800 bar the *Fd3m* structure is retained, but the set of the observed peaks shift to lower q values, indicating an increase in the lattice parameter. This is consistent with previous reported results on the effect of pressure on fully hydrated lyotropic systems.[4,7,9−11,66] As compared to temperature, the application of hydrostatic pressure has a countereffect owing to the significant influence on the conformational order of the hydrophobic tails of the investigated lipids (the same accounts of course for lipid/oil mixtures). The strength of this effect on lattice parameter changes was reported for fully hydrated systems of phospholipids and glycolipids[4,10] as follows: V_2 ($(\partial a/\partial P)_T$ can as big as 8 nm kbar^{-1}) > *Fd3m* (0.4 nm kbar^{-1} has been reported in one case[4]) > H_2 (values range from 0.1 to 0.6 nm kbar^{-1}) > L_α (less than 0.2 nm kbar^{-1}). We note that the extreme values observed sometimes for V_2 phases are due to anomalously strong swelling (high water uptake), and in these cases the effect of pressure on the lipid bilayers is somehow obscured. Nevertheless, it can be generally inferred that increasing pressure tends to induce structures with less negative interfacial curvatures, i.e., reducing the spontaneous curvature $|H_0|$ of the involved monolayers. Further, augmenting pressure increases both the bending rigidity κ of the membranes and the stiffness of the chains.[43] As a consequence, pressure enhances water uptake in the nonplanar phases from the surrounding excess water.[10,12,17,67] In this context, Pisani et al.[12] showed that increasing the pressure up to 1.8 kbar pushes the H_0 value of the fully hydrated MO system toward zero and strongly increases the ratio κ_G/κ from 0.14 to 1, in which κ_G is the monolayer splay modulus. They also found that compressing the MO-based *Pn3m* phase under full hydration condition by 1 kbar leads to a significant increase in the amount of solubilized water (the number of water molecules per MO increases from about 13 to 24).

The isothermal pressure dependence of the *Fd3m* lattice parameter is presented in Figure 3a. The lattice parameter strongly increases from 23.04 to 24.17 nm as the pressure varies in the range of 1−900 bar. This means that the lattice parameter increases ~1 Å for every 75 bar. Up to 900 bar, the response of the lattice parameter to pressure is linear, and the $(\partial a/\partial p)_T$ has a

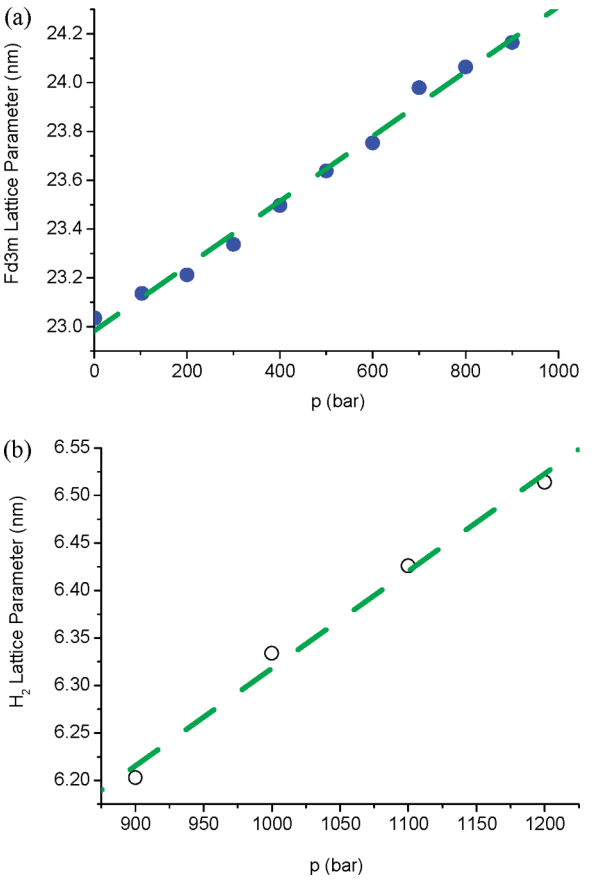

Figure 3. Isothermal pressure-dependence behavior of the lattice parameters of sample A: the *Fd3m* (a) and H_2 (b) phases. The lattice parameters for both nanostructures are extracted from the experiments displayed in Figure 1a.

value of ~1.33 nm kbar^{-1}. As mentioned in the Introduction, there is a limited number of studies carried out on characterizing the *Fd3m* phase. In one of these previous reports, it was found that the *Fd3m* phase based on saturated dialkyl xylolipid/water binary system[4] has $(\partial a/\partial p)_T$ of 0.4 nm kbar^{-1}. Thus, our present results reveal that the oil-loaded *Fd3m* phase is more pressure-sensitive. At 900 bar, the ternary system displays a coexistence of the *Fd3m* and the H_2 liquid crystalline nanostructures. On further compressing of the sample, the *Fd3m* phase vanishes, and we observe a direct structural transition to pure H_2 phase. As shown in Figure 3b, we witness a linear variation of the H_2 lattice parameter upon increasing pressure. This indicates most probably as mentioned above an increase in the order of the lipid and oil acyl chains (denser chain packing) and an enhancement of water uptake from the surrounding excess water. For the H_2 phase, the lattice parameter lies in the range of 6.20−6.51 nm, and the isothermal change, $(\partial a/\partial p)_T$, has a value of ~1.03 nm kbar^{-1}. This means that the lattice parameter increases ~1 Å for every 100 bar. In comparison, the present results imply that the impact of pressure on the oil-loaded *Fd3m* nanostructure is slightly greater than that of the H_2 phase.

The effect of pressure variation on the nanostructure of sample A was also studied at 7 °C (Figure 1b). Previous investigations carried out on ternary monoglycerides/oil/water mixtures showed that increasing the oil content at room temperature or increasing the temperature at a fixed oil concentration induces a transformation of the bicontinuous cubic nanostructure (*Pn3m* phase) via H_2 and *Fd3m* phases to a water-in-oil (W/O) microemulsion.[40,44] In accordance, sample A displays the occurrence of *Fd3m* → H_2

(66) Winter, R.; Czeslik, C. *Z. Kristallogr.* **2000**, *215*, 454–474.
(67) Narayan, O.; So, P. T. C.; Turner, D. C.; Gruner, S. M.; Tate, M. W.; Shyamsunder, E. *Phys. Rev. A* **1990**, *42*, 7479–7482.

structural transition, when decreasing the temperature at lower pressure values, and at relatively high pressures the formation of the V_2 nanostructure occurs. Carrying out the isotherm at lower temperature (7 °C), we found, as illustrated in Figure 1b, that the pressure increase in the range of 1−750 bar induces the *Fd3m* → H_2 → *Pn3m* structural transitions. At atmospheric pressure, the *Fd3m* phase is formed with a lattice parameter of 24.45 nm. The compression of the sample induces the formation of H_2 phase at ambient pressures, and then the formation of V_2 phase of the symmetry *Pn3m* is induced at pressures above 500 bar. The lattice parameter of this phase at 600 bar is ∼11.40 nm. Assuming that it has a linear isothermal change with increasing pressure, the $(\partial a/\partial p)_T$, has a value of ∼0.60 nm kbar^{-1}. It is worth comparing this value to those observed by Czeslik et al.[7] and Pisani et al.[12] for the fully hydrated MO system in the absence of oil. At ambient temperatures, they reported on the formation of V_2 phase of the symmetry *Pn3m*. According to their results, the $(\partial a/\partial p)_T$ values for the *Pn3m* phase were 0.73 (at 20 °C) and ∼0.43 nm kbar^{-1} (at 25 °C). Therefore, it can be concluded that the pressure-dependence behaviors of the oil-loaded H_2 and *Fd3m* phases are more sensitive than both oil-loaded and oil-free *Pn3m* phases. It is worth noting that increasing the TC content in ternary monoglycerides-based systems significantly decreases the solubilized water content.[40] Therefore, we believe that the temperature−pressure ($T-p$) behavior of the fully hydrated oil-loaded samples is strongly affected by the degree of water uptake during compressing the samples. In this regard, a possible reason in our study for having the values of $(\partial a/\partial P)_T$ in the order *Fd3m* > H_2 > V_2 is attributed to the less pronounced pressure-induced water uptake as that observed in other fully hydrated lipid/water systems (e.g., in the fully hydrated bicontinuous cubic phase based on phosphatidylethanolamines[4]).

To investigate the effect on the oil-loaded nanostructures during pressurization−depressurization changes, isothermal SAXS experiments were carried out on sample A at 17 °C (Figure 4). The investigated sample presents an example of the sensitivity of the oil-loaded nanostructure to the pressure history. It is clear that pressurization−depressurization variation induce the same structural transitions of *Fd3m* ↔ H_2 ↔ *Pn3m*. However, the phase transition boundaries and the lattice parameters are not fully reversible. For instance, the occurrence of the phase boundaries for the *Fd3m*−H_2 transition is mutually shifted for more than 100 bar. This boundary is the range of 800 < p < 850 bar during compressing the sample (Figure 4a), whereas it is in range of 600 < p < 700 bar in the reverse direction (Figure 4b). As shown in Figure 4c, also the lattice parameter of the H_2 phase in the pressurization direction is significantly different than that obtained during depressurizing the sample. It is most likely that the investigated system requires longer equilibration times during the (de)pressurization steps to obtain reversible nanostructures. In this context, one has also to take into consideration that structural transitions (such as *Pn3m* ↔ H_2), which involve significant change in the topology and water exchange inside−outside the self-assembled nanostructures, could require longer equilibration times.

Surprisingly, at higher pressures (above 800 bar in Figure 1a and at 350 bar in Figure 1b), we witness the appearance of an additional peak at q value of 3.46 nm^{-1} (it is marked with an asterisk having a d-spacing value of 1.81 nm), which is independent of the pressure variation. This distinct peak disappears during the pressure cycling as the pressure is reduced to less than 900 bar (data not shown). A possible explanation for the observation of this peak could be related to the pressure-induced ordering of the TC molecules. Most likely, part of the alkane

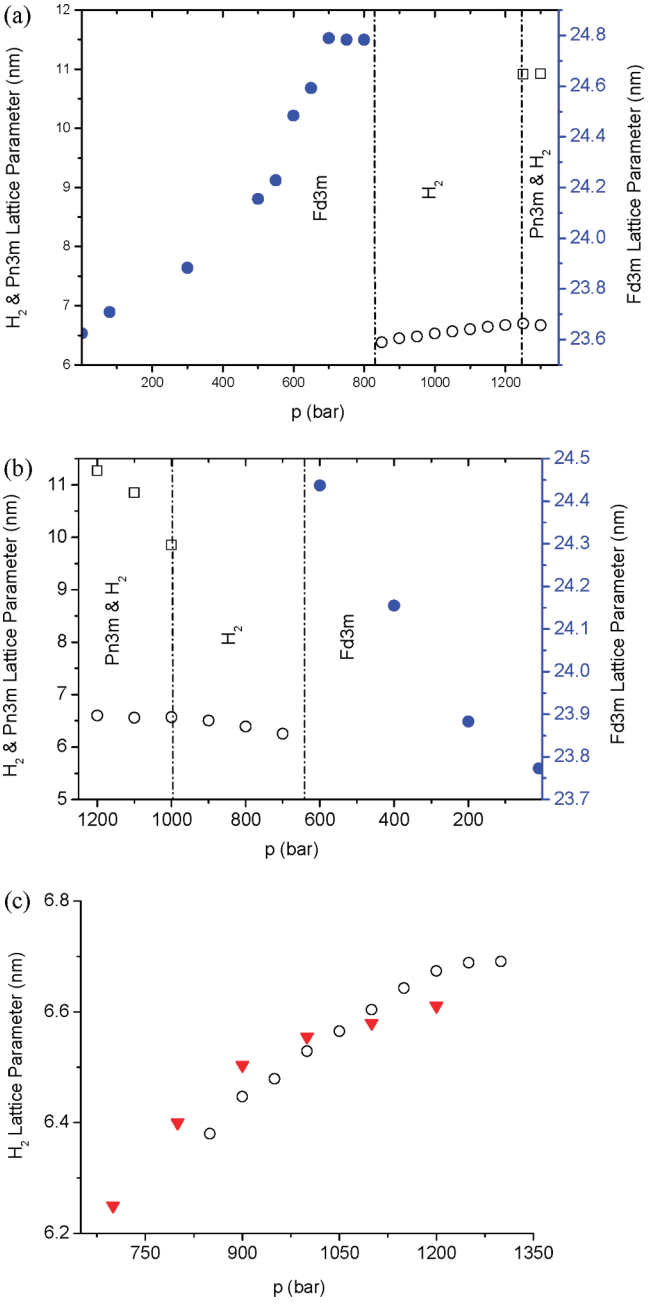

Figure 4. Isothermal pressure-dependence behavior of the lattice parameters of sample A at 17 °C. The effects of increasing pressure in the range of 1−1300 bar (a), and decreasing pressure values in the range of 1200−1 bar are displayed (b). The cubic *Pn3m*, the H_2, and the *Fd3m* phases are represented by open squares, open circles, and full circles, respectively. (c) For comparison, the effects of pressurization (open circles) and depressurization (full inverted triangles) on the lattice parameter of the H_2 phase are shown.

molecules begins to crystallize at high pressures and forms probably a triclinic structure. This claim is supported by the fact that the d-spacing value of this peak corresponds closely to that of the (001) reflection in the pure triclinic TC crystal as previously reported.[68,69]

2. Isobaric Behavior of Oil-Containing MO Systems. To monitor the isobaric structural transitions, samples A and B

(68) Nyburg, S. C.; Potworowski, J. A. *Acta Crystallogr., Sect. B: Struct. Sci.* **1973**, *B 29*, 347–352.
(69) Gilbert, E.; Reynolds, P.; White, J. *J. Appl. Crystallogr.* **2000**, *33*, 744–748.

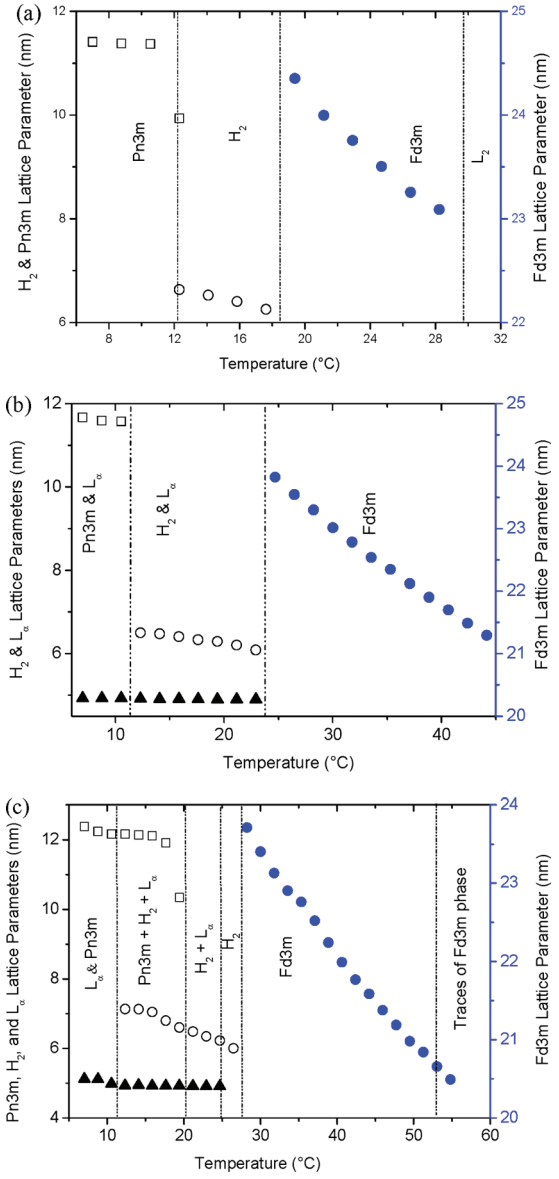

Figure 5. Isobaric temperature-dependence behavior of sample A at 750 (a), 1000 (b), and 1200 bar (c). The lattice parameters of the cubic *Pn3m*, the H_2, the L_α, and the *Fd3m* phases are represented by open squares, open circles, full triangles, and full circles, respectively. The dashed dot lines indicate the approximate phase boundaries between the different phases.

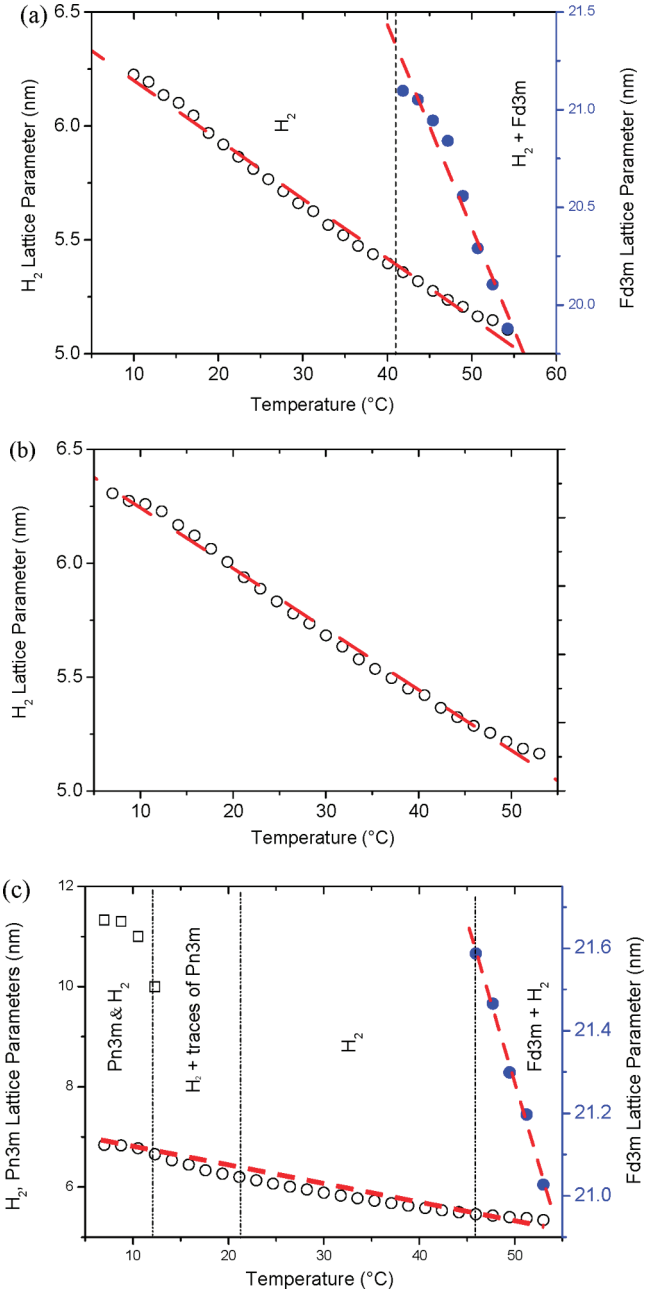

Figure 6. Isobaric temperature-dependence behavior of sample B at 44 (a), 285 (b), and 770 bar (c). The lattice parameters of the cubic *Pn3m*, the H_2, and the *Fd3m* phases are represented by open squares, open circles, and full circles, respectively. The dashed dot lines indicate the approximate phase boundaries between the different phases.

were investigated during temperature scans each at three different pressures. In Figures 5 and 6 the lattice parameter evolutions are presented for the different isobars. The trend of behavior in these two samples is similar: with increasing temperature, the lattice parameters of the observed nanostructures decrease. Thus, the opposite effect is observed as compared to the effect of pressure variations under isothermal conditions (see Introduction). However, as expected, the temperature-dependent behavior strongly depends on the system's nanostructure.

For sample A, as shown in Figure 5a, we detect at 750 bar a structural transition in the order of *Pn3m*→H_2→*Fd3m*→L_2 as the temperature increases in the range 7−53 °C. This structural pathway is in good agreement with previous results on the impact of temperature on TC-loaded MLO systems at atmospheric pressure.[40,44] Our results reveal that the strength of the temperature-dependent lattice parameter variations, $(\partial a/\partial T)_p$, in the formed liquid crystalline phases is ranked as follows: *Fd3m* > H_2 > *Pn3m* (Table 1). In the present report, we did not investigate the temperature-dependent behavior of the L_2 phase, but rather focused on the heating impact on the different ordered liquid crystalline phases. At 1 kbar, Figure 5b shows that increasing temperature in the range of 14−53 °C induces a transition from an L_α/H_2 biphasic state at low temperatures to a pure *Fd3m* phase. Selected scattering patterns from this experiment are presented in Figure 7a. Below 24.7 °C, the lattice parameter of the L_α nanostructure, having a value of 4.92 nm, does not show any significant change with increasing temperature. Remarkably at higher pressure (1.2 kbar), the compressed sample exhibits rich structural transformations (Figure 5c). Our results indicate in the temperature range

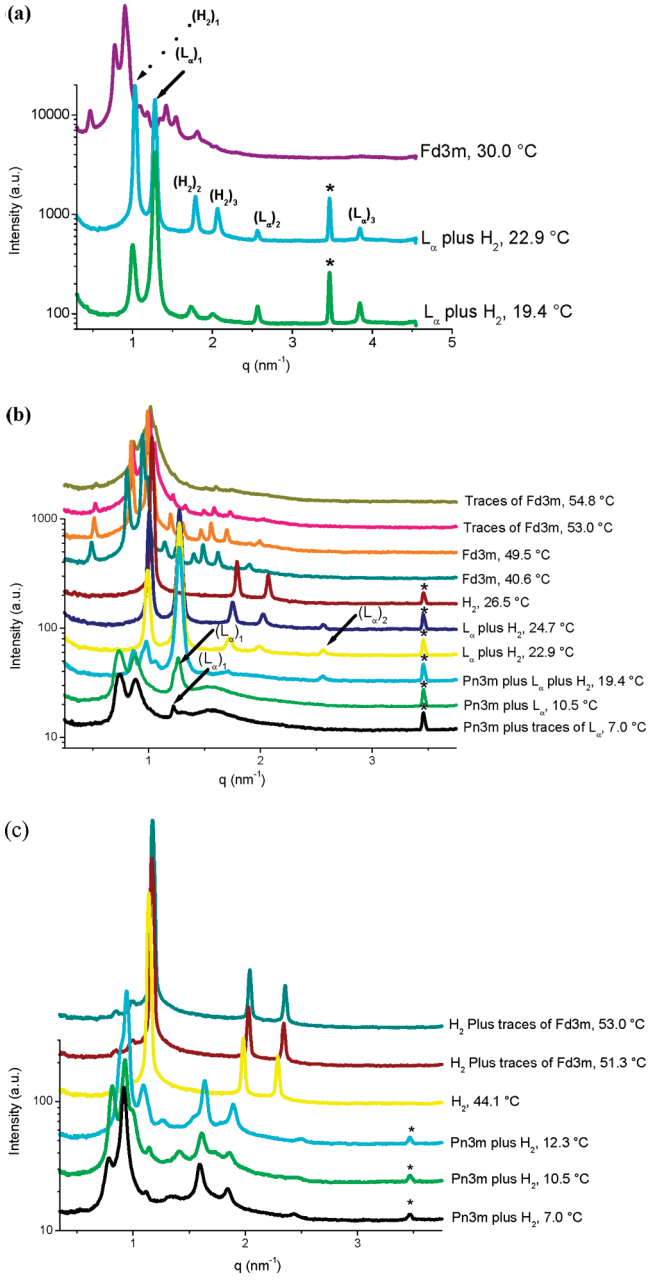

Figure 7. Selected SAXS scattering patterns from three different isobars. Representative examples from sample A are taken for the isobaric experiments, which were carried out at 1000 (a) and 1200 bar (b). Panel (c) shows selected SAXS scattering patterns for sample B at six different temperatures at 770 bar. The scattering curves in this figure are shifted by an arbitrary constant for better visibility.

7−56.6 °C transitions in the following order: (*Pn3m* + L_α) → (*Pn3m* + L_α + H_2) → (L_α + H_2) → H_2 → *Fd3m* → traces of *Fd3m* coexisting with L_2. Selected scattering patterns at different temperatures are presented in Figure 7b. Peak shape analysis of the stronger diffraction peaks in the *Fd3m* phase from 41 to 55 °C show that peak widths remain nearly constant, even though above 53 °C the peak intensities strongly reduce, which means that the *Fd3m* phase begins to destabilize and induces the formation of the L_2 system. Thus, in this region, the experimental findings simply imply the occurrence of a biphasic region: the L_2 phase is dominant but coexisting with small amounts of well-ordered *Fd3m* domains.

In Figures 5a,c, the temperature-dependent behavior of the *Pn3m* phase is similar. At low temperatures, the lattice parameter of the pure *Pn3m* is ∼11.4 at 750 bar and 12.3 nm at 1.2 kbar. The $(\partial a/\partial T)_{750\ bar}$ is relatively small and has a value of ∼−0.018 nm °C^{-1} as the temperature increases from 7 to 10.5 °C (Figure 5a), whereas at higher pressure $(\partial a/\partial T)_p$ is about −0.026 nm °C^{-1} as temperature increases from 7 to 15.9 °C (Figure 5c). These values compare well to that found at high temperatures in the oil-free MO/water system[7] and also to the temperature-dependent behavior of surfactant peptide-loaded MO-based *Pn3m* phases published in our recent report[26] (both studies reported at atmospheric pressure an $(\partial a/\partial T)_p$ value of ∼−0.02 nm °C^{-1}). Further, our present results indicate a significant decrease to occur near the *Pn3m*−H_2 transition boundary (Figures 5a,c). This sudden deviation could be attributed to the significant change in the topology occurring during the transition from *Pn3m* to H_2 phase. In particular, this transition involves a relatively strong expulsion of water from the hydrophilic channels of the bicontinuous cubic phase into the surrounding aqueous medium.[40,70] In this context, it should be stressed that $a(T)$ of the fully hydrated *Pn3m* phase in the binary MO/water system[7] at atmospheric pressure remains nearly constant in the temperature range of 5−30 °C and then decreases abruptly with an initial rate of −0.089 nm °C^{-1}. A similar temperature behavior of the *Pn3m* phase was also found in the aqueous dispersion of dioleoylphosphatidylethanolamine (DOPE).[71]

In Figures 5a−c, all $a(T)_p$ for the H_2 and *Fd3m* phases at the three different pressures display a linear change with varying temperature. The values of $(\partial a/\partial T)_p$ are given in Table 1. The lattice parameters of the H_2 and *Fd3m* phases show a relatively big temperature dependence displaying $(\partial a/\partial T)_p$ values in the range of −0.039 to −0.084 and −0.119 to −0.142 nm °C^{-1}, respectively. For comparison, the MO-based H_2 phase in the absence of oil[7] is less temperature-sensitive: $(\partial a/\partial T)_p$ = −0.017 nm °C^{-1}. Also, a rather small effect was approved in the phosphatidylcholine/lauric acid/water mixtures ($(\partial a/\partial T)_p$ = −0.006 nm °C^{-1}).[11]

A second example of the temperature-dependent structural transitions was obtained for sample B containing less oil. For this sample, different isobars were studied at pressures values of 44, 285, and 770 bar (Figure 6). At 44 bar, a temperature scan from 10 to 53 °C induces a structural transition of H_2 → H_2 + *Fd3m* (Figure 6a). In the investigated temperature range, our results reveal that the H_2 is stabilized at a higher pressure (Figure 6b). It can also clearly be seen that the H_2 phase extends over a remarkable large region in panels a−c of Figure 6. At 770 bar, we detect as shown in Figure 6c the following transitions: (*Pn3m* + H_2) → H_2 → (H_2 + traces of *Fd3m*). Figure 7c presents selected scattering patterns for these transitions. Above 46 °C, two additional weak peaks are detectable at approximately 0.85 and 0.99 nm^{-1}, respectively. It could indicate the coexistence of the H_2 phase with traces of *Fd3m* phase, since the indexing of these peaks is consistent with the reflections (220) and (311) of an *Fd3m* phase. In addition, this assumption is supported by the temperature-induced coexistence of H_2 with *Fd3m* at lower pressures (Figure 7c).

The lattice parameters of the H_2 and *Fd3m* phases show a linear temperature-dependent isobaric behavior with $(\partial a/\partial T)_p$ values in the range of −0.026 to −0.034 and −0.079 to −0.104 nm °C^{-1}, respectively. These results indicate that the *Fd3m* phase shows a similar isobaric behavior to that observed in sample A (higher oil content), and again, it is significantly more temperature sensitive than the H_2 phase.

(70) Squires, A.; Templer, R. H.; Ces, O.; Gabke, A.; Woenckhaus, J.; Seddon, J. M.; Winter, R. *Langmuir* **2000**, *16*, 3578–3582.
(71) Erbes, J.; Czeslik, C.; Hahn, W.; Winter, R.; Rappolt, M.; Rapp, G. *Ber. Bunsenges. Phys. Chem.* **1994**, *98*, 1287–1293.

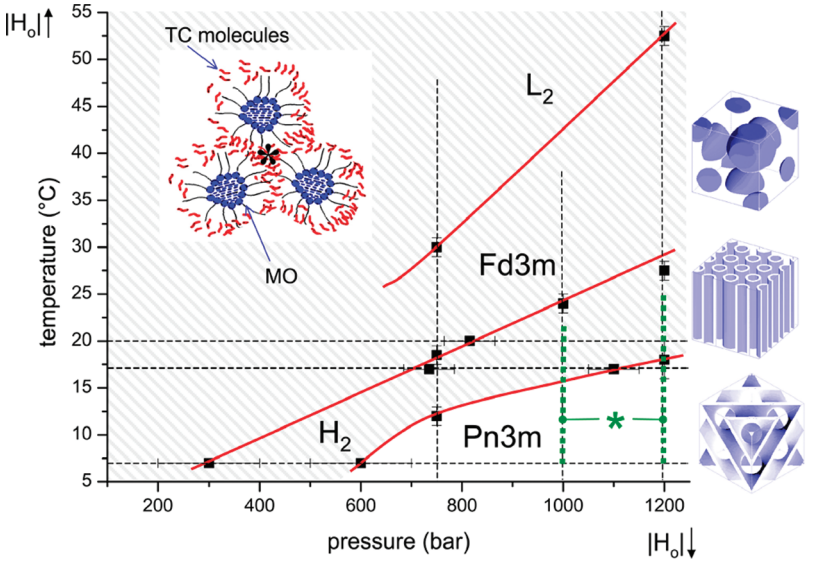

Figure 8. Temperature−pressure ($T-p$) behavior of the fully hydrated TC-loaded MO/water system. All performed isobars and isotherms (dashed lines) from sample A were used to construct a partial $p-T$ phase diagram and to estimate ($\partial T_t/\partial p$) values. Discontinuous membrane phase regions (including L_2, *Fd3m*, and H_2 phases) are highlighted with a gray background. The green asterisk marks the biphasic regions (bold green dotted lines) apparent as the oil-loaded samples compressed at pressure values in the range of 1.0−1.2 kbar: the L_α phase coexists with the *Pn3m* as well as to some extent also with the H_2 phase. As demonstrated in the scheme of the L_2 phase, TC especially helps to overcome packing limitation in the discontinuous mesophases because it is a perfect filler of interstitial regions (∗). The structural electron density schemes for the *Pn3m*, H_2, and *Fd3m* phase have been adopted from previous studies.[42,57]

Table 1

sample	nanostructure	temp range (°C) at isobaric condition	$(\partial a/\partial T)_p$ (nm °C^{-1})	pressure range (bar) at isothermal conditions	$(\partial a/\partial p)_T$ (nm kbar^{-1})
A	*Pn3m*	7.0−10.5 (at 750 bar)	−0.018	600−750	0.60 (at 7 °C)
	H_2	12.3−17.6 (at 750 bar)	−0.071	1−900	1.03 (at 20 °C)
	Fd3m	19.4−28.2 (at 750 bar)	−0.142	900−1200	1.33 (at 20 °C)
	L_2	> 28.2 (at 750 bar)			
	L_α	10.1−22.9 (at 1 kbar)	−0.002		
	H_2	14.1−22.9 (at 1 kbar)	−0.039		
	Fd3m	24.7−53.0 (at 1 kbar)	−0.119		
	Pn3m	7.0−15.9 (at 1.2 kbar)	−0.026		
	L_α	7.0−24.7 (at 1.2 kbar)	−0.020		
	H_2	12.3−24.7 (at 1.2 kbar)	−0.084		
	Fd3m	28.2−51.3 (at 1.2 kbar)	−0.125		
	traces of *Fd3m*	53.0−61.9 (at 1.2 kbar)			
B	H_2	10.0−52.5 (at 44 bar)	−0.026		
	Fd3m	> 40.0 (at 44 bar)	−0.104		
	H_2	7.0−53.0 (at 285 bar)	−0.027		
	Pn3m	7.0−10.54 (at 770 bar)	−0.012		
	H_2	7.0−53.0 (at 770 bar)	−0.034		
	traces of *Fd3m*	> 46.0 (at 770 bar)	−0.079		

Similar to the isothermal changes (Figure 1), we detect here also an additional peak at high q value (Figure 7, ∗). At high pressures and low temperatures, it appears at 3.46 nm^{-1} and vanishes with increasing temperature. As mentioned above in the first section, it is most likely that the observation of this peak is related to partial TC crystallization. Depressurization and heating prevent this phenomenon.

3. $p-T$ Phase Diagram of Oil-Containing MO Systems. All experiments carried out on sample A are summarized in the $p-T$ phase diagram of Figure 8. At the transition boundary between the H_2 and *Fd3m* phases, we obtained a (dT_t/dp) value of ∼23.0 °C kbar^{-1} (Figure 8), which is in good agreement with that of Duesing et al.[4] for a glycolipid/water system (27.5 °C kbar^{-1}). The phase boundary gradient involving the *Pn3m* and H_2 phases is estimated in the linear regime to be about 13 °C kbar^{-1}. For comparison, assuming the lattice constant along *Pn3m* to H_2 phase boundary to be the same, a transition slope of 33 °C kbar^{-1} was estimated for the binary MO/water system.[7] The slope for the *Fd3m*−L_2 transition can be only very roughly estimated, since in general we found no sharp transition from the *Fd3m* to L_2 phase (Figures 5c and 7b). However, at least we can conclude that the (dT_t/dp) slope has an approximate value of 50 °C kbar^{-1}, and thus it is the biggest (to the best of our knowledge no literature data are available on this transition), and hence, the obtained data suggest that the *Fd3m*−L_2 is the strongest pressure-dependent transition.

The pressure dependence of the lipid phase transition temperatures (T_t) can be predicted[10,15,17] from the Clapeyron equation

$$\frac{dT_t}{dP} = \frac{\Delta V_m}{\Delta S_m} = \frac{T_t \Delta V_m}{\Delta H_m} \quad (1)$$

where ΔV_m, ΔS_m, and ΔH_m are the changes of the molar transition volume, the molar transition entropy, and the

molar transition enthalpy, respectively. This equation predicts a linear behavior between the pressure and the transition temperature as ΔV_m and ΔS_m having the same pressure dependence or being independent of pressure variations. Experimental findings reveal linearity in this relationship[4,10,15] at least with compressing different lipid samples up to 2 kbar. In the absence of oil, the $Pn3m-H_2$ transition[7] for MO in excess water occurs at approximately T_t value of 95 °C having very small ΔH_m and ΔS_m values of 0.3 kJ mol^{-1} and 0.8 J °C^{-1} mol^{-1}, respectively. Assuming in the present study that the oil-loaded system has also a small ΔH_m value similar to that previously found in the absence of oil,[7] the slight pressure-dependent effect could be attributed to correspondingly a small change in the ΔV_m value. As predicted from Clapeyron equation, the fluid−fluid structural transitions with a small enthalpy (entropy) changes have the tendency of having also a correspondingly smaller volume changes, and therefore, the pressure dependence of the transition temperatures have small changes.[10] Previous experimental findings on fluid−fluid structural transitions indicated such slight impact. For instance, Duesing et al.[4] found that the pressure dependence of the transition temperatures in different fully hydrated phospholipid and glycolipid systems for $L_\alpha-V_2$, $L_\alpha-H_2$, $Pn3m-H_2$, and H_2-Fd3m lies within a narrow range of 20−30 °C kbar^{-1}.

A simple approach to understand the effects of temperature and pressure on self-assembled nanostructures is given by the concept of the critical packing parameter (CPP), which is defined as

$$v_s/a_0 l \quad (2)$$

where v_s is the hydrophobic chain volume, a_0 is the headgroup area, and l is the hydrophobic chain length.[72] It is well-known that an increase in the temperature[2,5,26,40,73] reduces the value of a_0 due to the headgroup's dehydration, and it enhances simultaneously the value of v_s. This means that temperature induces a monotonously decrease in the monolayer thickness and the water core radii. Therefore, it promotes the formation of phases with greater negative spontaneous curvature. The addition of an oil also induces the formation of monolayers with negative spontaneous curvature ($H_0 < 0$). As expected, our present results demonstrate that heating the oil-loaded samples leads to an increase of the CPP value, and thus it extends the H_2 and the $Fd3m$ regions. Conversely, compressing the samples[4,7,10,12] increases simultaneously the values of l (acyl chain stretching) and decreases the v_s value (denser acyl chain packing). This effect decreases the CPP value, and thus it explains the tendency to form V_2 and, even more, to induce the planar phase, L_α, at high pressures. However, the large extension of the discontinuous phase region (H_2, $Fd3m$, and L_2) by addition of oil (Figure 8, shaded area) is not fully explainable with taking into consideration the CPP concept alone. While the main driving force for inducing stronger membrane bending basis on curvature frustration release,[74] the main energy barrier for the formation of discontinuous phases such as the H_2 or L_2 phases is given by packing limitations.[51,75] These effects are widely overcome when oil is of assistance to fill out the interstitial regions in the hydrophobic matrix, and hence the discontinuous lipid phases are strongly stabilized.

Conclusions

In this study, the $p-T$ behavior of fully hydrated TC-loaded MO phases was determined from synchrotron SAXS data. The investigations were done in temperature and pressure ranges of 7−62 °C and 1−1200 bar, respectively. To fully understand the behavior of these oil-loaded nanostructures, it was important comparing our findings with those of the fully hydrated oil-free MO and MLO systems reported in previous studies.[5,7] Under the same experimental conditions (same p and T ranges), both the fully hydrated MO and MLO systems[5,7] solely self-assemble in the cubic $Pn3m$ phase; i.e., the H_2 phase is only induced at elevated temperatures (at ambient pressure, the $Pn3m-H_2$ transition temperature of the fully hydrated MO is ∼95 °C). However, our present results reveal that the $p-T$ phase behavior in the presence of oil (Figure 8) displays the $Pn3m$ to H_2 boundary at much lower temperatures and higher pressures, respectively. Further, the formations of the discontinuous $Fd3m$ cubic phase as well as the inverted micellar L_2 phase are recorded over wide p and T ranges. As expected, this $p-T$ behavior strongly depends on the oil content.

The observed isothermal variations of the lattice parameters for the different formed nanostructures during compression (Table 1) indicate a pressure-dependent sensitivity in the order of $Fd3m > H_2 > Pn3m$. Quantitatively, we observed an increase in the lattice parameters of the $Fd3m$ phase of 1 Å per 75 bar, for the H_2 phase an increase of ∼1 Å per 100 bar, and for the $Pn3m$ phase an increase of 1 Å per 170 bar. Further, pressurization−depressurization changes induce the same structural transitions in both directions; however, the structures are not readily reversible but exhibit rather big hysteresis as indicated by shifted phase boundaries and significant differences in the corresponding lattice parameters. The samples require most probably longer equilibration times during the (de)compression, and thus the isothermal reversibility would most probably be achieved by applying slower scan rates.

Our data clearly demonstrate that the temperature and the pressure sensitivity of oil-loaded MO aggregates is especially enhanced for both the H_2 and the $Fd3m$ phases, whereas for the $Pn3m$ phase the estimated values of $(\partial a/\partial T)_p$ and $(\partial a/\partial p)_T$ are satisfactorily similar to those published for fully hydrated oil-free MO system.[7] In this context, the obtained $(\partial T_t/\partial p)_a$ values for the different observed phase boundaries are the following: ∼13 °C/kbar for the H_2-Pn3m, ∼23 °C/kbar for the H_2-Fd3m, and roughly 50 °C/kbar for the $Fd3m-L_2$ boundary. Therefore, for oil-loaded MO systems, it appears that the $Fd3m-L_2$ phase boundary under full hydration conditions displays not only the steepest gradient, but it is also significantly steeper as compared to any other transition boarder previously reported for different fully hydrated phospholipid and glycolipid systems.[4,10] The $(dT_t/dp)_a$ values[4,10] for the $L_\alpha-V_2$, the $L_\alpha-H_2$, the $Pn3m-H_2$, and the H_2-Fd3m phases boundaries lie within a narrow range of 20−30 °C kbar^{-1}. Since the $Fd3m$ to L_2 transition involves no great topology changes and also most probably the amount of solubilized water does not change dramatically, it is most likely that the high stability of the $Fd3m$ phase is due to the minimized packing energy, when oil is present. On the other hand, a relatively high value of $(dT_t/dp)_a$ of 44 °C kbar^{-1} was also previously reported for another transition involving significant changes in structure and water transfer: the $L_\alpha-H_2$ in DOPE-based aqueous dispersion.[17] This makes clear that both packing and bending energies are of outmost importance in modulating the stability of fully hydrated nonlamellar phases.

(72) Isrealachvilli, J. N.; Mitchell, D. J.; Ninham, B. W. *J. Chem. Soc., Faraday Trans. 2* **1976**, *72*, 1525–1568.
(73) Geil, B.; Feiweier, T.; Pospiech, E. M.; Eisenblatter, J.; Fujara, F.; Winter, R. *Chem. Phys. Lipids* **2000**, *106*, 115–126.
(74) Mares, T.; Daniel, M.; Perutkova, S.; Perne, A.; Dolinar, G.; Iglic, A.; Rappolt, M.; Kralj-Iglic, V. *J. Phys. Chem. B* **2008**, *112*, 16575–16584.
(75) Kozlov, M. M.; Leikin, S.; Rand, R. P. *Biophys. J.* **1994**, *67*, 1603–1611.